Slip Flow and Convective Heat Transfer of The Carreau Fluid Over a Radially Stretching Sheet

G. Radha[1], N. Bhaskar Reddy[1], K. Gangadhar[2*] and S. Sudhakar Reddy[3]
[1]*Dept of mathematics, S.V. University, Tirupati, A.P., India.*
[2]*Dept. of mathematics, ANU Ongole Campus, Ongole-523001, Andhra Pradesh, India*
[3]*Dept. of Mathematics, Sri Venkateswara Engineering College for Women, Tirupati, A.P.*

Abstract:
The prime objective of present exploration is to study effects of velocity slip and convective heating on an incompressible two dimensional axisymmetric flow of the Carreau fluid over a radially stretching sheet. The Carreau constructive model is used to discuss the characteristics of both Shear-thinning and Shear- thickening fluids. The momentum equations for the two-dimensional field are first modeled for Carreau fluid with the aid of the boundary layer approximations obtained system of boundary layer equations is converted into ordinary differential equations with high linearity using appropriate transformations. Numerical solutions via fourth order Runge-Kutta method along with shooting technique are obtained and deliberated accordingly. Discussions of graphs pertaining different prominent parameters is also added. Numerical values of skin friction coefficient and local Nusselt number are also given and well deliberated. It is noted that higher values of the slip parameters, the velocity field and skin friction coefficient are reduced. Moreover, temperature field is as increasing function of Biot number.
Key words: *Axisymmetric flow, Carreau fluid, radially stretching sheet, velocity slip, convective condition.*

Nomenclature

c_p – Specific heat at constant pressure (*J/kg K*)
f – Dimensionless stream function
u - Velocity component in x-direction (*m/s*)
v - Velocity component in y-direction (*m/s*)
T - Temperature of the fluid (^0C)
T_f - Temperature at the stretching surface
T_∞ - Ambient fluid temperature
u_w - Stretching velocity along x – direction
Re - Local Reynolds number
q_w - Surface heat flux
L_1 - Slip length
h_f - convective heat transfer coefficient
Bi – convective heat transfer parameter
m – stretching parameter
C_f - Skin friction coefficient along xdirection
Nu - Local Nusselt number
q_w - Surface heat flux
Pr – Prandtl number
Re - Local Reynolds number

Greek symbols

k - Thermal conductivity (W/m K)
μ - Thermal viscosity (*N s/m*)
ρ -Fluid density (kg/m^3)
$\nu = \mu / \rho$ - Kinematic viscosity of the fluid
η – Similarity variable
γ - momentum slip parameter
θ - Non-dimensional temperature

Subscript

w – Condition at the surface
∞ - Condition at infinity

Super script

$'$ - Differentiation with respect to η

1. Introduction:

It is a well-known fact that stretching flows have received considerable attention in recent times due to their demand in practical applications (aerodynamic extrusion of plastic sheets, cooling of metallic sheets or electronic chips, crystallization of liquid films during condensation, hot rolling of metals, etc.). Extensive investigations of the boundary layer flow over a plane stretching sheet have been already performed. However, the literature survey reveals that rare studies regarding an axisymmetric flow over a radially stretching sheet are available. The classical problem of an axisymmetric flow induced by a stretching sheet was discussed by Ariel [1] who found exact, perturbed, asymptotic, and numerical solutions for the problem. Exact and differential numerical solutions for an axisymmetric flow over a radially stretching sheet with partial slip effects were also reported by Ariel [2]. Sahoo [3] studied the slip effects on an axisymmetric flow of an electrically conducting viscoelastic fluid over a surface stretched with a linear velocity in the radial direction. Shahzad et al. [4] showed the existence of an exact solution for a steady axisymmetric flow due to a nonlinearly stretching sheet (the velocity of the stretching sheet is proportional to x^3). Analytical and numerical solutions were recently computed by Ali et al. [5] for an axisymmetric flow of an electrically conducting viscous fluid in the presence of slip effects over a nonlinearly stretching sheet in the radial direction.

The interest in flows of non-Newtonian fluids with heat transfer has grown substantially in recent years because such flows are extensively used in engineering and industrial applications (nuclear fuel slurries, oil recovery, food processing, paper production, glass blowing, plastic sheet formation, and extrusion of polymeric fluids and melts). Specifically, the boundary layer flows of non-Newtonian fluids are of special importance. A few studies in this direction can be found in [6] for relevant issues related to the behavior and modeling of non-Newtonian fluids. There are many non-Newtonian fluid models, e.g., the power-law model, Ellis model, Carreau model, and Bingham model [6]. Being used to describe a shear-thickening fluid, the power-law viscosity model yields a zero effective value of the "apparent viscosity" for small shear rates. Almost all fluids possess a finite, though very small, viscosity even if the velocity shear is very small in the outer region of the flow (i.e., the region outside the boundary layer). Hence, a viscosity model that gives a constant, albeit small, value for the apparent viscosity for the shear rate tending toward zero would better conform to the behavior of a real fluid. However, little interest has been paid to such models for the fluid viscosity with these properties, though they are widely used in chemical engineering. The constitutive model proposed by Carreau [7] involves four additional parameters in comparison to the Newtonian case and, thus, can describe the rheology of a wide range of non-Newtonian fluids. This model fits reasonably well in many flow situations, in particular, for some dilute, aqueous, and polymer solutions and also melts. The first theoretical study of a creeping flow of the Carreau model fluid around a sphere was performed by Chhabra and Uhlherr [8]. Using the velocity variational principle, they obtained an estimation of the upper bound of the drag coefficient of a sphere. Their theoretical results are in good agreement with their experimental ones and also with the numerical results of Bush and Phan-Thien [9]. Khan and Hashim [10] have been numerically investigated the axisymmetric flow and heat transfer analysis of the Carreau fluid over a radially stretching sheet.

In numerous engineering and chemical procedures like paper production, thinning and annealing of copper wires, glass fiber and hot rolling, significance of heat and mass transfer is evident. That is why researchers are motivated to explore new avenues in this hot area [11–15]. In continuation, Ibrahim and Haq [16] examined MHD stagnation point of a viscous

nanofluid flow with convective boundary condition. Rahman et al. [17] discussed flow of a nanofluid over an exponential stretching sheet with convective boundary condition on surface using Buongiorno's model. Ramzan et al. [18] analytically studied micropolar fluid flow through a porous sheet with effects of thermal radiation, Joule heating and magneto hydrodynamic (MHD) in attendance of partial slip and convective boundary condition. Waqas et al. [19] explored micropolar fluid flow past a nonlinear stretching sheet with magnetohydrodynamics (MHD), viscous dissipation, mixed convection and Joule heating in the presence of convective boundary condition. Ramzan et at. [20] studied the MHD flow of a radioactive Jeffery nanofluid flow with the effects of convective heat and mass boundary conditions.

The main focus of the present study is a numerical investigation of an axisymmetric boundary layer flow of the Carreau fluid induced by a radially stretching sheet under the influence of velocity slip and convective condition. The mathematical model is based on a system of non-linear differential equations under the boundary layer assumptions; obtained system of boundary layer equations is converted into ordinary differential equations with high linearity using appropriate transformations, which are then solved numerically by the fourth order Runge – Kutta method along with shooting technique. Finally, several interesting effects of the power law index n, weissenberg number We slip parameter γ, Biot number Bi and prandtl number $\Pr$ on the velocity and temperature profiles are discussed. To the best of our information such a problem has not been solved yet.

2.1 Governing equations:

The mass conservation and linear momentum equations governing a steady flow of an incompressible fluid can be written as

$\operatorname{div} V = 0,$

$\rho (V \nabla) V = -\nabla p + \operatorname{div} S$,

Where V is the velocity vector, ρ is the density of the fluid, p is the pressure, and S is the extra stress tensor. The extra stress tensor S for an incompressible Carreau fluid is

$S = \mu_1 A_1$, $\mu = \mu_1\left(\dot{\gamma}\right)$,

Where $A_1 = \nabla V + (\nabla V)^T$ is the strain rate tensor, $\mu_1\left(\dot{\gamma}\right)$ is the generalized Newtonian viscosity, and

$$\dot{\gamma} = \sqrt{tr\left(A_1^2\right)/2} \quad , \qquad (1)$$

Where tr stands for the trace.

The generalized viscosity for the Carreau model is described by the following formula [7]:

$$\mu = \mu_\infty + (\mu_0 - \mu_\infty)\left[1 + \left(\Gamma \dot{\gamma}\right)^2\right]^{(n-1)/2} .$$

Here n is the power –law index (the fluid is said to be shear-thinning for $0< n <1$, shear-thinning for $n >1$, and Newtonian for $n =1$); μ_∞ and μ_0 are the infinite-shear-rate and zero-shear-rate viscosities, and Γ is the material time constant often referred to as the "relaxation time." In what follows, we use the equation of state at $\mu_\infty = 0$:

$$\mu = \mu_0 \left[1 + \left(\Gamma \dot{\gamma} \right)^2 \right]^{(n-1)/2}$$

For mathematical modeling, we take a cylindrical polar coordinate system (r, θ, z). For an axisymmetric flow, we have $\partial / \partial \theta = 0$. For a two-dimensional axisymmetric flow, the velocity vector is presented as

$$V = [u(r,z), 0, w(r,z)] \tag{2}$$

Where u and w are the velocity components along the radial directions, respectively.
In view of Eq. (2), Eq. (1) becomes

$$\dot{\gamma} = \left[2\left(\frac{\partial u}{\partial r} \right)^2 + 2\left(\frac{\partial w}{\partial z} \right)^2 + \left(\frac{\partial u}{\partial z} + \frac{\partial w}{\partial r} \right)^2 + \frac{2u^2}{r^2} \right]^{1/2}$$

Under the above-mentioned assumptions, the system of the differential equations of the problem is written as

$$\frac{\partial u}{\partial r} + \frac{u}{r} + \frac{\partial w}{\partial z} = 0 \tag{3}$$

$$\rho\left(u \frac{\partial u}{\partial r} + w \frac{\partial u}{\partial z} \right) = -\frac{\partial p}{\partial r} + \frac{\partial S_{rr}}{\partial r} + \frac{\partial S_{rz}}{\partial z} + \frac{S_{rr} - S_{\theta\theta}}{r} \tag{4}$$

$$\rho\left(u \frac{\partial w}{\partial r} + w \frac{\partial w}{\partial z} \right) = -\frac{\partial p}{\partial z} + \frac{1}{r}\frac{\partial}{\partial r}(r S_{rz}) + \frac{\partial S_{zz}}{\partial z} \tag{5}$$

Here

$$S_{rr} = 2\mu_0 \frac{\partial u}{\partial r} \left\{ 1 + \Gamma^2 \left[2\left(\frac{\partial u}{\partial r} \right)^2 + 2\left(\frac{\partial w}{\partial z} \right)^2 + \left(\frac{\partial u}{\partial z} + \frac{\partial w}{\partial r} \right)^2 + \frac{2u^2}{r^2} \right] \right\}^{(n-1)/2}$$

$$S_{\theta\theta} = 2\frac{u}{r}\mu_0 \left\{ 1 + \Gamma^2 \left[2\left(\frac{\partial u}{\partial r} \right)^2 + 2\left(\frac{\partial w}{\partial z} \right)^2 + \left(\frac{\partial u}{\partial z} + \frac{\partial w}{\partial r} \right)^2 + \frac{2u^2}{r^2} \right] \right\}^{(n-1)/2}$$

$$S_{zz} = 2\mu_0 \frac{\partial w}{\partial z} \left\{ 1 + \Gamma^2 \left[2\left(\frac{\partial u}{\partial r} \right)^2 + 2\left(\frac{\partial w}{\partial z} \right)^2 + \left(\frac{\partial u}{\partial z} + \frac{\partial w}{\partial r} \right)^2 + \frac{2u^2}{r^2} \right] \right\}^{(n-1)/2} \tag{6}$$

$$S_{rz} = \mu_0 \left(\frac{\partial u}{\partial z} + \frac{\partial w}{\partial r} \right) \left\{ 1 + \Gamma^2 \left[2\left(\frac{\partial u}{\partial r} \right)^2 + 2\left(\frac{\partial w}{\partial z} \right)^2 + \left(\frac{\partial u}{\partial z} + \frac{\partial w}{\partial r} \right)^2 + \frac{2u^2}{r^2} \right] \right\}^{(n-1)/2}$$

Substitution of the expressions for $S_{rr}, S_{\theta\theta}, S_{zz}$ and S_{rz} (4) into Eqs. (3) Yields

$$\begin{aligned} \rho\left(u \frac{\partial u}{\partial r} + w \frac{\partial u}{\partial z} \right) = & -\frac{\partial p}{\partial r} + \mu_0 \left[\frac{\partial^2 u}{\partial r^2} + \frac{\partial^2 u}{\partial z^2} + \frac{\partial}{\partial r}\left(\frac{u}{r} \right) \right] \\ & \times \left\{ 1 + \Gamma^2 \left[2\left(\frac{\partial u}{\partial r} \right)^2 + 2\left(\frac{\partial w}{\partial z} \right)^2 + \left(\frac{\partial u}{\partial z} + \frac{\partial w}{\partial r} \right)^2 + \frac{2u^2}{r^2} \right] \right\}^{(n-1)/2} \\ & + 2\mu_0 \frac{\partial u}{\partial r}\frac{\partial}{\partial r} \left\{ 1 + \Gamma^2 \left[2\left(\frac{\partial u}{\partial r} \right)^2 + 2\left(\frac{\partial w}{\partial z} \right)^2 + \left(\frac{\partial u}{\partial z} + \frac{\partial w}{\partial r} \right)^2 + \frac{2u^2}{r^2} \right] \right\}^{(n-1)/2} \\ & + \mu_0 \left(\frac{\partial u}{\partial z} + \frac{\partial w}{\partial r} \right) \frac{\partial}{\partial z} \left\{ 1 + \Gamma^2 \left[2\left(\frac{\partial u}{\partial r} \right)^2 + 2\left(\frac{\partial w}{\partial z} \right)^2 + \left(\frac{\partial u}{\partial z} + \frac{\partial w}{\partial r} \right)^2 + \frac{2u^2}{r^2} \right] \right\}^{(n-1)/2} \end{aligned} \tag{7}$$

$$\rho\left(u\frac{\partial u}{\partial r}+w\frac{\partial u}{\partial z}\right)=-\frac{\partial p}{\partial z}+\mu_0\left(\frac{\partial^2 w}{\partial r^2}+\frac{\partial^2 w}{\partial z^2}\right)$$
$$\times\left\{1+\Gamma^2\left[2\left(\frac{\partial u}{\partial r}\right)^2+2\left(\frac{\partial w}{\partial z}\right)^2+\left(\frac{\partial u}{\partial z}+\frac{\partial w}{\partial r}\right)^2+\frac{2u^2}{r^2}\right]\right\}^{(n-1)/2}$$
$$+2\mu_0\frac{\partial w}{\partial z}\frac{\partial}{\partial z}\left\{1+\Gamma^2\left[2\left(\frac{\partial u}{\partial r}\right)^2+2\left(\frac{\partial w}{\partial z}\right)^2+\left(\frac{\partial u}{\partial z}+\frac{\partial w}{\partial r}\right)^2+\frac{2u^2}{r^2}\right]\right\}^{(n-1)/2} \quad (8)$$
$$+\mu_0\left(\frac{\partial u}{\partial z}+\frac{\partial w}{\partial r}\right)\frac{\partial}{\partial r}\left\{1+\Gamma^2\left[2\left(\frac{\partial u}{\partial r}\right)^2+2\left(\frac{\partial w}{\partial z}\right)^2+\left(\frac{\partial u}{\partial z}+\frac{\partial w}{\partial r}\right)^2+\frac{2u^2}{r^2}\right]\right\}^{(n-1)/2}$$
$$+\frac{\mu_0}{r}\frac{\partial w}{\partial r}\left\{1+\Gamma^2\left[2\left(\frac{\partial u}{\partial r}\right)^2+2\left(\frac{\partial w}{\partial z}\right)^2+\left(\frac{\partial u}{\partial z}+\frac{\partial w}{\partial r}\right)^2+\frac{2u^2}{r^2}\right]\right\}^{(n-1)/2}$$

At $n=1$ and $\Gamma=0$, Eqs. (5) transform to those of the Newtonian fluid.
We introduced the dimensionless variables

$$u^*=\frac{u}{U},\quad w^*=\frac{w}{U},\quad r^*=\frac{r}{L},\quad z^*=\frac{z}{L},\quad p^*=\frac{p}{\rho U^2}$$

(L and U are the characteristic length and stretching velocity, respectively). In view of the above-introduced dimensionless variables, Eqs. (5) becomes

$$u^*\frac{\partial u^*}{\partial r^*}+w^*\frac{\partial u^*}{\partial z^*}=-\frac{\partial p^*}{\partial r^*}+\varepsilon_1\left[\frac{\partial^2 u^*}{\partial r^{*2}}+\frac{\partial^2 u^*}{\partial z^{*2}}+\frac{\partial}{\partial r^*}\left(\frac{u^*}{r^*}\right)\right]$$
$$\times\left\{1+\varepsilon_2\left[2\left(\frac{\partial u^*}{\partial r^*}\right)^2+2\left(\frac{\partial w^*}{\partial z^*}\right)^2+\left(\frac{\partial u^*}{\partial z^*}+\frac{\partial w^*}{\partial r^*}\right)^2+\frac{2u^{*2}}{r^{*2}}\right]\right\}^{(n-1)/2}$$
$$+2\varepsilon_1\frac{\partial u^*}{\partial r^*}\frac{\partial}{\partial r^*}\left\{1+\varepsilon_2\left[2\left(\frac{\partial u^*}{\partial r^*}\right)^2+2\left(\frac{\partial w^*}{\partial z^*}\right)^2+\left(\frac{\partial u^*}{\partial z^*}+\frac{\partial w^*}{\partial r^*}\right)^2+\frac{2u^{*2}}{r^{*2}}\right]\right\}^{(n-1)/2} \quad (9)$$
$$+\varepsilon_1\left(\frac{\partial u^*}{\partial z^*}+\frac{\partial w^*}{\partial r^*}\right)\frac{\partial}{\partial z^*}\left\{1+\varepsilon_2\left[2\left(\frac{\partial u^*}{\partial r^*}\right)^2+2\left(\frac{\partial w^*}{\partial z^*}\right)^2+\left(\frac{\partial u^*}{\partial z^*}+\frac{\partial w^*}{\partial r^*}\right)^2+\frac{2u^{*2}}{r^{*2}}\right]\right\}^{(n-1)/2}$$

$$u^*\frac{\partial u^*}{\partial r^*}+w^*\frac{\partial u^*}{\partial z^*}=-\frac{\partial p^*}{\partial z^*}+\varepsilon_1\left(\frac{\partial^2 w^*}{\partial r^{*2}}+\frac{\partial^2 w^*}{\partial z^{*2}}\right)$$

$$\times\left\{1+\varepsilon_2\left[2\left(\frac{\partial u^*}{\partial r^*}\right)^2+2\left(\frac{\partial w^*}{\partial z^*}\right)^2+\left(\frac{\partial u^*}{\partial z^*}+\frac{\partial w^*}{\partial r^*}\right)^2+\frac{2u^{*2}}{r^{*2}}\right]\right\}^{(n-1)/2}$$

$$+2\varepsilon_1\frac{\partial w^*}{\partial z^*}\frac{\partial}{\partial z^*}\left\{1+\varepsilon_2\left[2\left(\frac{\partial u^*}{\partial r^*}\right)^2+2\left(\frac{\partial w^*}{\partial z^*}\right)^2+\left(\frac{\partial u^*}{\partial z^*}+\frac{\partial w^*}{\partial r^*}\right)^2+\frac{2u^{*2}}{r^{*2}}\right]\right\}^{(n-1)/2} \qquad (10)$$

$$+\varepsilon_1\left(\frac{\partial u^*}{\partial z^*}+\frac{\partial w^*}{\partial r^*}\right)\frac{\partial}{\partial r^*}\left\{1+\varepsilon_2\left[2\left(\frac{\partial u^*}{\partial r^*}\right)^2+2\left(\frac{\partial w^*}{\partial z^*}\right)^2+\left(\frac{\partial u^*}{\partial z^*}+\frac{\partial w^*}{\partial r^*}\right)^2+\frac{2u^{*2}}{r^{*2}}\right]\right\}^{(n-1)/2}$$

$$+\frac{\varepsilon_1}{r^*}\frac{\partial w^*}{\partial r^*}\left\{1+\varepsilon_2\left[2\left(\frac{\partial u^*}{\partial r^*}\right)^2+2\left(\frac{\partial w^*}{\partial z^*}\right)^2+\left(\frac{\partial u^*}{\partial z^*}+\frac{\partial w^*}{\partial r^*}\right)^2+\frac{2u^{*2}}{r^{*2}}\right]\right\}^{(n-1)/2}$$

Where ε_1 and ε_2 are the dimensionless parameters:

$$\varepsilon_1=\frac{\mu_0/\rho}{LU} \qquad \varepsilon_2=\frac{\Gamma^2}{(LU)^2} \quad .$$

In the standard boundary layer approximation, we use the following estimates. In this analysis, it is assumed that $O(u)=1, O(r)=1$, and $O(p)=1$, while w and z are the order of $\delta: O(w)=\delta=O(z)$. In addition, the dimensional parameters ε_1 and ε_2 are of the order of $\delta^2: O(\varepsilon_1)=\delta^2=O(\varepsilon_2)$ (δ is the boundary layer thickness).

Accordingly, Eqs. (6) are simplified and can be cast as

$$u^*\frac{\partial u^*}{\partial r^*}+w^*\frac{\partial u^*}{\partial z^*}=-\frac{\partial p^*}{\partial r^*}+\varepsilon_1\frac{\partial^2 u^*}{\partial z^{*2}}\left[1+\varepsilon_2\left(\frac{\partial u^*}{\partial z^*}\right)^2\right]^{(n-1)/2}+\varepsilon_1\left(\frac{\partial u^*}{\partial z^*}\right)\frac{\partial}{\partial z^*}\left[1+\varepsilon_2\left(\frac{\partial u^*}{\partial z^*}\right)^2\right]^{(n-1)/2},$$

$$0=-\frac{\partial p^*}{\partial z^*} \quad . \qquad (11)$$

In the dimensional form, Eqs. (7) becomes

$$u\frac{\partial u}{\partial r}+w\frac{\partial u}{\partial z}=-\frac{1}{\rho}\frac{\partial p}{\partial r}+\nu\frac{\partial^2 u}{\partial z^2}\left[1+\Gamma^2\left(\frac{\partial u}{\partial z}\right)^2\right]^{(n-1)/2}+\nu\frac{\partial u}{\partial z}\frac{\partial}{\partial z}\left[1+\Gamma^2\left(\frac{\partial u}{\partial z}\right)^2\right]^{(n-1)/2}$$

$$0=-\frac{1}{\rho}\frac{\partial p}{\partial z} \qquad (12)$$

Where $\nu=\mu_0/\rho$ is the kinematic viscosity.

2.2 Formulation of the problem:

We consider an axisymmetric two-dimensional flow of an incompressible Carreau fluid induced by a radially stretching sheet. The sheet is located in the plane $z=0$, and the fluid resides in the half-space z > 0. The sheet is stretched in its own plane with a power-law velocity $U=br^m$ in the radial direction. The sheet surface is maintained at a constant convective temperature T_f and the ambient fluid temperature T_∞ ($T_f > T_\infty$) .

In this problem, the flow is preferably generated by the stretching sheet and the pressure gradient does not affect a flow filed.

Under these assumptions, the governing problem for a forced convective boundary layer flow is return as

$$\frac{\partial u}{\partial r}+\frac{u}{r}+\frac{\partial w}{\partial z}=0 \tag{13}$$

$$u\frac{\partial u}{\partial r}+w\frac{\partial u}{\partial z}=\nu\frac{\partial^2 u}{\partial z^2}\left[1+\Gamma^2\left(\frac{\partial u}{\partial z}\right)^2\right]^{(n-1)/2}+\nu(m-1)\Gamma^2\left(\frac{\partial u}{\partial z}\right)^2\frac{\partial^2 u}{\partial z^2}\left[1+\Gamma^2\left(\frac{\partial u}{\partial z}\right)^2\right]^{(n-3)/2} \tag{14}$$

$$u\frac{\partial T}{\partial r}+w\frac{\partial T}{\partial z}=\alpha\frac{\partial^2 T}{\partial z^2} \tag{15}$$

$$z=0\ ,\quad u=U+L\frac{\partial u}{\partial z}=br^m+L\frac{\partial u}{\partial z},\quad w=0\ ,\quad -k\frac{\partial T}{\partial z}=h_f(T_f-T) \tag{16}$$

$$z\to\infty:\qquad u\to 0\ ,\quad T\to T_\infty \tag{17}$$

Where $\alpha=k/(\rho c_p)$, c_p is the specific heat, k is the thermal conductivity, L is the slip length, $m>0$ is the stretching parameter, h_f is the wall heat transfer coefficient and T is the fluid temperature.

Let us introduce the local similarity transformations

$$\psi(r,z)=-r^2U\ \mathrm{Re}^{-1/2}\ f(\eta),\quad \theta(\eta)=\frac{T-T_\infty}{T_f-T_\infty},\qquad \eta=\frac{z}{r}\mathrm{Re}^{1/2} \tag{18}$$

In which $\psi(r,z)$ is the Stokes stream function and $\mathrm{Re}=rU/\nu$ is the local Reynolds number. In view of Eqs. (8),

$$u=Uf'(\eta)\qquad w=-U\ \mathrm{Re}^{-1/2}\left(\frac{m+3}{2}f(\eta)+\frac{m-1}{2}\eta f'(\eta)\right) \tag{19}$$

and the governing equations of the problem are written as

$$\left[1+nWe^{\,2}(f'')^2\right]\left[1+We^{\,2}(f'')^2\right]^{(n-3)/2}f'''+\left[\frac{m+3}{2}\right]ff''-m(f')^2=0 \tag{20}$$

$$\theta''+\left[\frac{(3+m)}{2}\right]\mathrm{Pr}\ f\theta'=0\ ; \tag{21}$$

$$f(0)=0\ ,\quad f'(0)=1+\gamma\ f''(0)\ ,\quad \theta'(0)=-Bi\ (1-\theta(0))\ ; \tag{22}$$

$$f'(\infty)\to 0\ ,\quad \theta(\infty)\to 0\ . \tag{23}$$

Here $We=\left(b^3\Gamma^2r^{3m-1}/\nu\right)^{1/2}$ is the local Weissenberg number, $\gamma=\frac{L}{r}\mathrm{Re}^{1/2}$ is the velocity slip parameter, $Bi=\frac{h_f}{r}\mathrm{Re}^{1/2}$ is the local Biot number and $\mathrm{Pr}=\mu_0c_p/k$ is the Prandtl number. The local wall shear stress and local surface heat flux are described by the following expression:

$$\tau_w=\mu_0\frac{\partial u}{\partial z}\left\{\left[1+\Gamma^2\left(\frac{\partial u}{\partial z}\right)^2\right]^{(n-1)/2}\right\}_{z=0}\qquad q_w=-k\left(\frac{\partial T}{\partial z}\right)_{z=0} \tag{24}$$

Using τ_w and q_w, we can write the local skin friction coefficient C_f and the local number as

$$C_f=\frac{T_W}{\rho U^2}\ ,\qquad Nu=\frac{rq_w}{k(T_w-T_\infty)}\ ; \tag{8}$$

$$\mathrm{Re}^{1/2} C_f = f''(0)\left[1 + We^{2}\left(f''(0)\right)^{2}\right]^{(n-1)/2}, \qquad \mathrm{Re}^{-1/2} Nu = -\theta'(0) \tag{25}$$

3. Solution of the Problem:

The reduced set of coupled ordinary differential equations (20) - (21) subject to the boundary conditions (22) - (23) are highly nonlinear in nature. Hence, it is very difficult possess a closed form analytical solution. Therefore, it has been solved numerically by fourth order Runge-Kutta-Fehlberg integration scheme with the help of algebraic software Mat lab. The algorithm in Mat lab has been well tested for its accuracy and robustness. Thus, this has been used to solve a wide range of non-linear problems. In this method, we choose a finite value of $\eta \to \infty$ as η_{10} in such a way that the boundary conditions are satisfied asymptotically. Table 1 depicts the validation of the present results by comparison with the existed results for some restricted cases (Khan and Hashim [10]). We noticed that the comparison shows smart agreement for every value of η, which conform that the present results are accurate. For numerical results, we considered the non dimensional parameter values as $\gamma = Bi = 0.2, We = 3, m = \mathrm{Pr} = 1$. These values are kept as common in the entire study except the variations in respective figures.

Table 1 Comparison of Nusselt number $\mathrm{Re}_x^{-1/2} Nu_x$ with the available results in literature for different values of n for m=1, We = 3, Pr = 1 and $Bi \to \infty$.

	$\mathrm{Re}_x^{-1/2} Nu_x$	
n	Present results	Khan and Hashim [10]
0.5	0.752804	0.752 802
1.0	0.851992	0.851 995
1.5	0.910006	0.910 010
2.0	0.946571	0.946 575

4 Results and Discussion:

The main aim of the present section is to characterize the effects of various physical parameters like Biot number, power law index parameter, local Weissenberg number, Prandtl number, slip parameter. Hence, figs 2, 3, 4, 5, and 6 have been plotted for such objective.

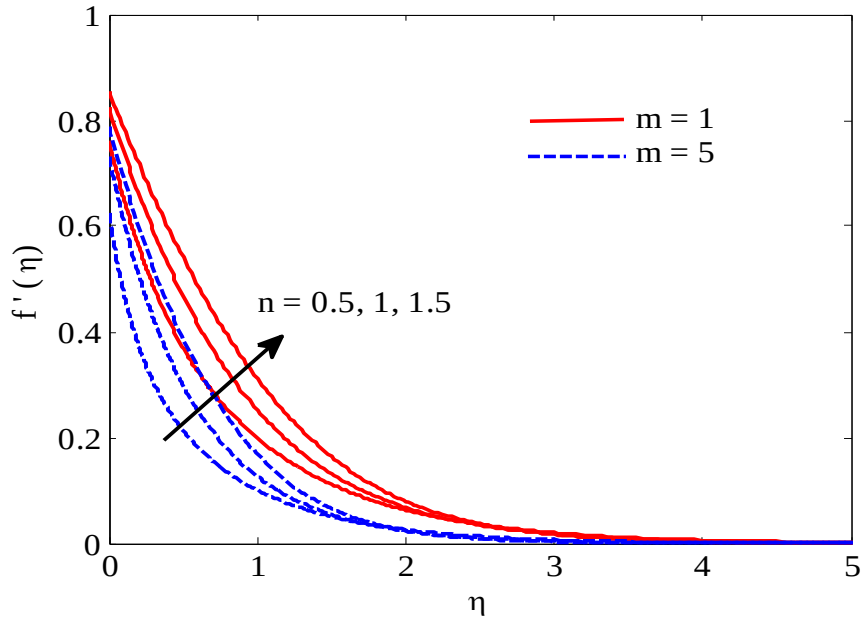

Figure 2a: Velocity profiles for various values of *n* for *We* = 3, *Pr* = 1, γ = *Bi* = 0.2: *m* = 1 (Solid curve) and *m* = 5 (Dashed curve).

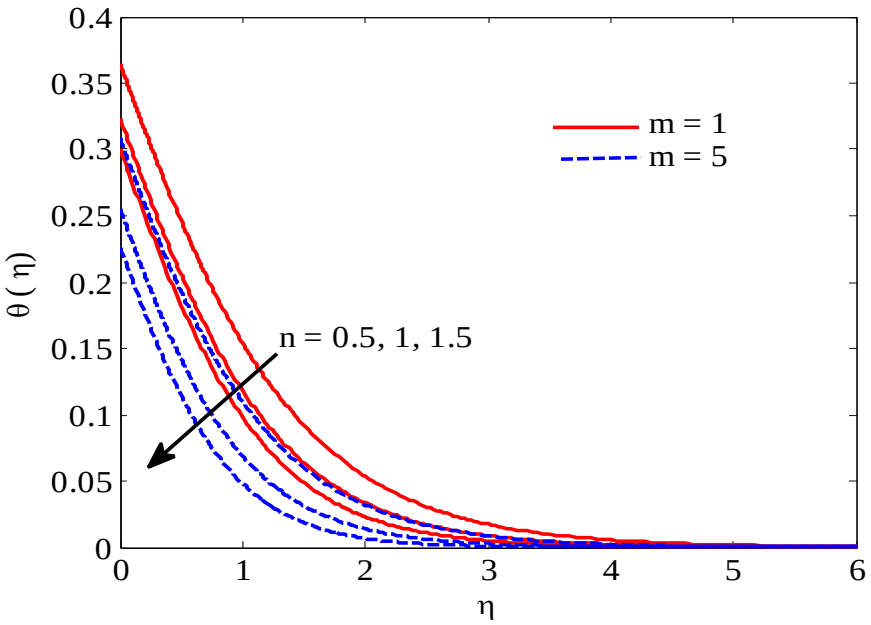

Figure 2b: Temperature profiles for various values of *n* for *We* = 3, *Pr* = 1, γ = *Bi* = 0.2: *m* = 1 (Solid curve) and *m* = 5 (Dashed curve).

Figure 2 is plotted to visualize the effects of power law index parameter on velocity $f'(\eta)$ and temperature $\theta(\eta)$ profiles for $m = 1$ and $m = 5$ respectively. As m increases, the fluid velocity and the momentum boundary layer thickness are seen to decrease for shear thinning $(n = 0.5)$, Newtonian $(n = 1)$ and shear thickening $(n = 1.5)$ fluids. The momentum boundary layer thickness in the shear thinning fluid is smaller than that in the shear thickening fluid. From figure 2b, that fluid temperature and thermal boundary layer thickness are seen to be decreases with an increase in both stretching parameter m and power law index parameter n .

The thermal boundary layer thickness in the shear thickening fluids is lower than that in the shear thinning fluids.

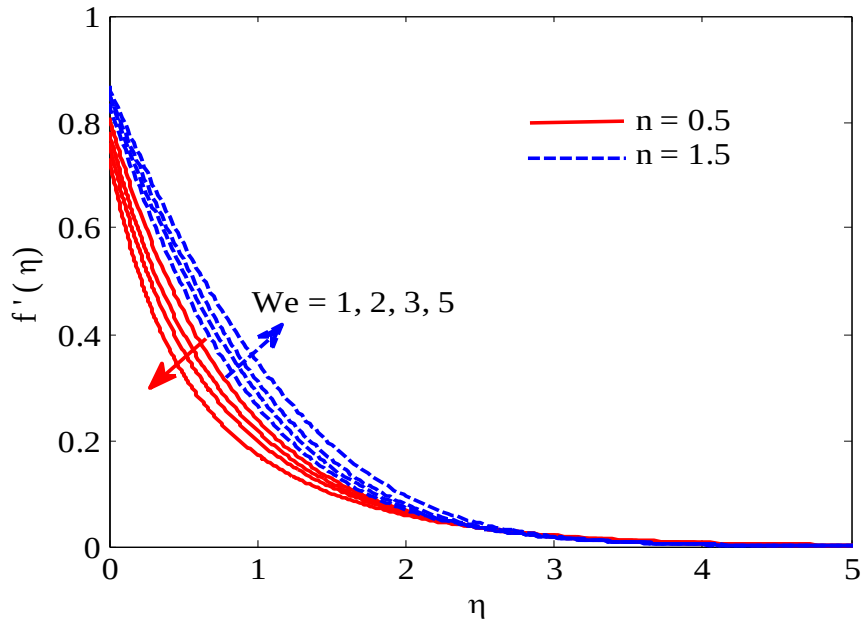

Figure 3a: Velocity profiles for various values of *We* for $m = 1$, $Pr = 1$, $\gamma = Bi = 0.2$: $n = 0.5$ (Solid curve) and $n = 1.5$ (Dashed curve).

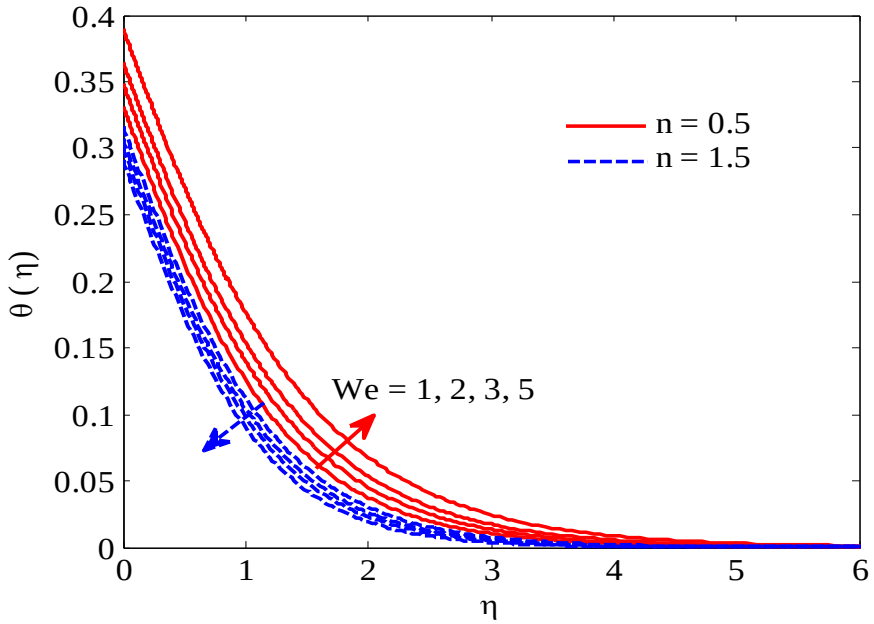

Figure 3b: Temperature profiles for various values of *We* for $m = 1$, $Pr = 1$, $\gamma = Bi = 0.2$: $n = 0.5$ (Solid curve) and $n = 1.5$ (Dashed curve).

Figure 3 shows the dependences $f'(\eta)$ and $\theta(\eta)$ for the shear thinning $(n = 0.5)$ and shear thickening $(n = 1.5)$ for different values of the Weissenberg number We . It is observed from the figure 3a that an increase in the Weissenberg number decreases the velocity of the shear thinning fluid and increases the velocity of the shear thickening fluid. It is seen in fig. 3b that the temperature distribution of the shear thinning fluid increases with increasing Weissenberg number, whereas the temperature of the shear thickening fluid decreases. Figure 4 shows the

dependence $f'(\eta)$ and $\theta(\eta)$ for the shear thinning $(n = 0.5)$ and shear thickening $(n = 1.5)$ for different values of the slip parameter γ. It follows from fig 4a that an increase in the slip parameter decreases the fluid velocity for both shear thinning and shear thickening fluid. It is seen in fig 4b that the temperature of the fluid increases with an increase in γ for both shear thinning and shear thickening fluid.

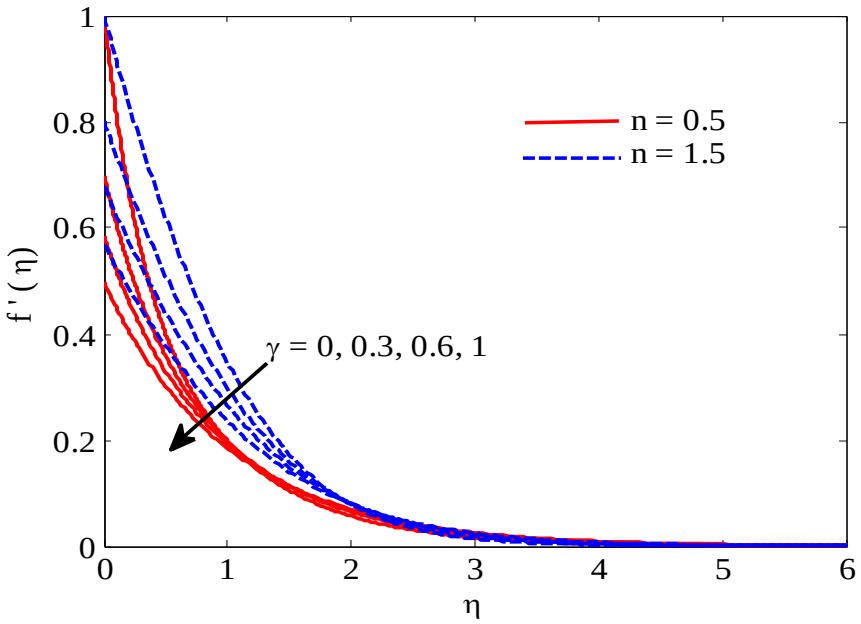

Figure 4a: Velocity profiles for various values of γ for m = 1, We = 3, Pr = 1, Bi = 0.2: n = 0.5 (Solid curve) and n = 1.5 (Dashed curve).

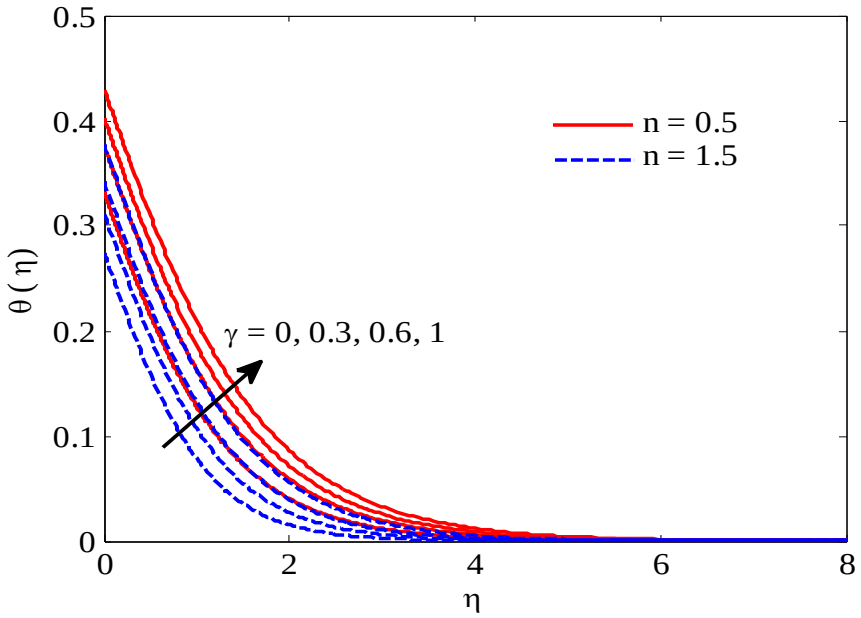

Figure 4b: Temperature profiles for various values of γ for m = 1, We = 3, Pr = 1, Bi = 0.2: n = 0.5 (Solid curve) and n = 1.5 (Dashed curve).

Figure 5 shows the dependence $\theta(\eta)$ for the shear thinning $(n = 0.5)$ and shear thickening $(n = 1.5)$ fluids for various values o the Prandtl number $\Pr$ .It is observed that the temperature decreases with increasing Prandtl number fluids with lower Prandtl numbers possess higher thermal conductivities. Therefore, the heat can diffuse from the wall faster in fluids with lower Prandtl numbers. Hence the Prandtl number can be used to increase the rate of cooling in conducting flows. In addition, an increase in the Prandtl number corresponds to reduction of the thermal boundary layer thickness. Furthermore, it is observed that the effect of the Prandtl number is more noticeable for the shear thinning fluid as compared to the shear thickening fluid.

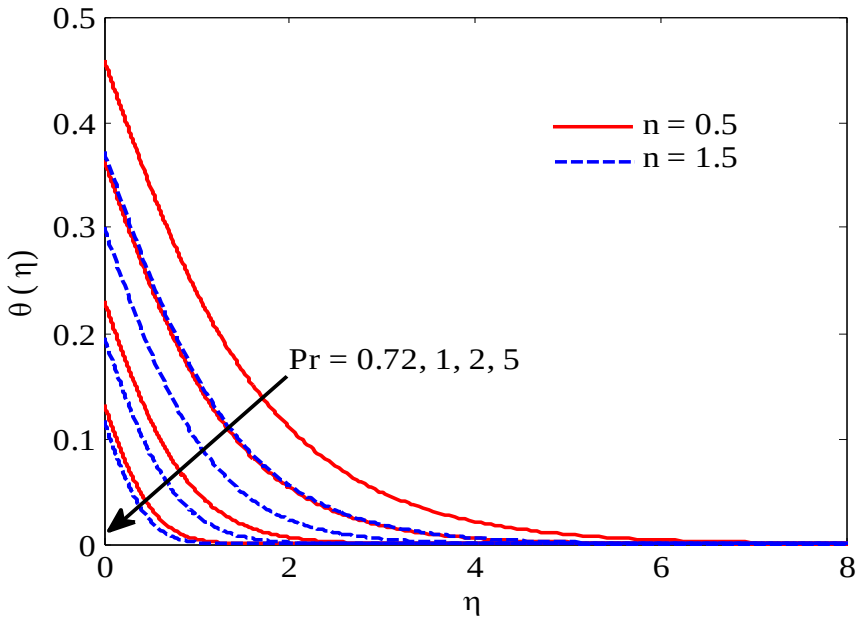

Figure 5: Temperature profiles for various values of *Pr* for *m* = 1, *We* = 3, γ = *Bi* = 0.2: *n* = 0.5 (Solid curve) and *n* = 1.5 (Dashed curve).

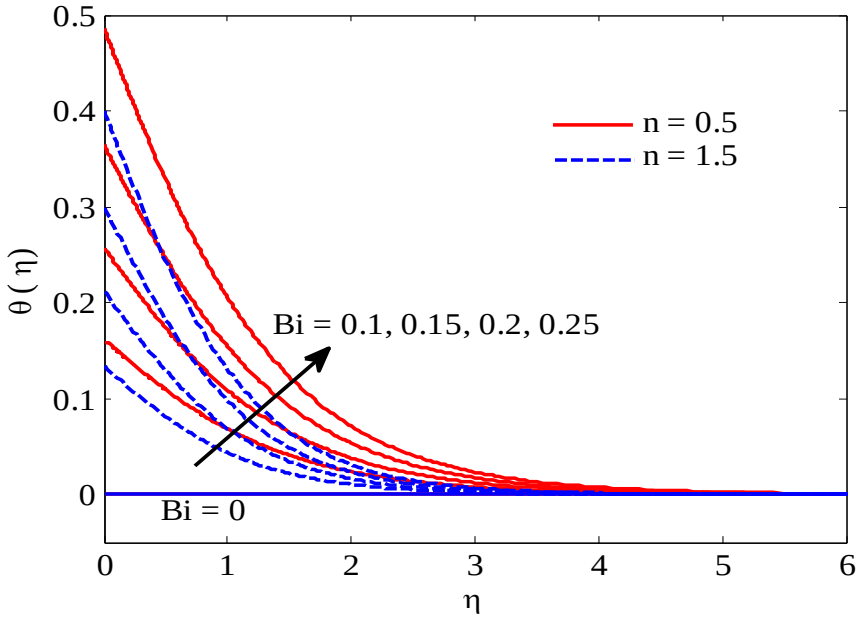

Figure 6: Temperature profiles for various values of *Bi* for *m* = 1, *We* = 3, *Pr* = 1, γ = 0.2: *n* = 0.5 (Solid curve) and *n* = 1.5 (Dashed curve).

Figure 6 elucidate that temperature with concomitant boundary layer thickness are increased with larger values of Biot number Bi. The Biot number Bi have high dependency on heat transfer coefficient h_f. Larger heat transfer coefficient corresponds to higher values of temperature. This ruling lead to increasing values of temperature profile for larger values of Biot number.

Table 2 skin friction coefficient $-\mathrm{Re}_x^{1/2} C_f$ for different values of the parameters *n*, *m* and *We*.

n	m	We	γ	$-\mathrm{Re}_x^{1/2} C_f$
0.5	1	2	0.2	0.701948
1	1	2	0.2	0.878425
1.5	1	2	0.2	1.028695
2	1	2	0.2	1.161001
0.5	2	2	0.2	0.786489
0.5	3	2	0.2	0.842618
0.5	4	2	0.2	0.883978
0.5	5	2	0.2	0.916393
0.5	1	3	0.2	0.618505
0.5	1	4	0.2	0.558616
0.5	1	5	0.2	0.513902
0.5	1	6	0.2	0.479061
0.5	1	2	0.3	0.637350
0.5	1	2	0.4	0.586813
0.5	1	2	0.5	0.545510
0.5	1	2	0.6	0.510742

Table 3 Nusselt number $\mathrm{Re}_x^{-1/2} Nu_x$ for different values of the parameters *n*, *m*, *We*, γ , *Bi* and *Pr*.

n	m	We	γ	Bi	Pr	$\mathrm{Re}_x^{-1/2} Nu_x$
0.5	1	2	0.2	0.2	1	0.156372
1	1	2	0.2	0.2	1	0.158913
1.5	1	2	0.2	0.2	1	0.160564
2	1	2	0.2	0.2	1	0.161723
0.5	2	2	0.2	0.2	1	0.158040
0.5	3	2	0.2	0.2	1	0.159576
0.5	4	2	0.2	0.2	1	0.160945
0.5	5	2	0.2	0.2	1	0.162160
0.5	1	3	0.2	0.2	1	0.154841
0.5	1	4	0.2	0.2	1	0.153550
0.5	1	5	0.2	0.2	1	0.152449
0.5	1	6	0.2	0.2	1	0.151490
0.5	1	2	0.3	0.2	1	0.155278
0.5	1	2	0.4	0.2	1	0.154324
0.5	1	2	0.5	0.2	1	0.153467
0.5	1	2	0.6	0.2	1	0.152683
0.5	1	2	0.2	0.3	1	0.211490
0.5	1	2	0.2	0.4	1	0.256739

0.5	1	2	0.2	0.5	1	0.294550
0.5	1	2	0.2	0.6	1	0.326618
0.5	1	2	0.2	0.2	2	0.169806
0.5	1	2	0.2	0.2	3	0.175612
0.5	1	2	0.2	0.2	4	0.179021
0.5	1	2	0.2	0.2	5	0.181323

The variation of the local skin friction coefficient and the local Nusselt number for different problem parameters are displayed in tables 2 and 3 respectively. It is seen that the local skin friction coefficient increases with an increment in the power law index n and stretching parameter m. Further, we can see from table 2 that the local skin friction coefficient decreases with an increase in the Weissenberg number We and slip parameter γ. For fixed vales of $\Pr$, We, m, γ and Bi the local Nusselt number increases with an increase in the power law index n (see table 3). The local Nusselt number is an increasing function of the Prandtl number $\Pr$, stretching parameter m and Biot number Bi on the other hand; it is also noticed from table 3 that the local Nusselt number decreases with an increase in the Weissenberg number we and slip parameter γ.

5. Conclusions:

We have examined are incompressible two dimensional axisymmetric flow of the Carreau fluid under the influence of velocity slip and convective condition. The main points of this investigation can be summarized as follows.

1) The fluid velocity and the momentum boundary layer thickness increases with an increase in power law index. The reverse trend is observed for the temperature field.

2) An increase in slip parameter leads to decrease in both the fluid velocity and the momentum boundary layer thickness.

3) The temperature field and rate of heat transfer increases with an increase in local Biot number.

4) The local Nusselt number increased with an increase in Prandtl number. The local Nusselt number in the Shear thinning fluid decreases with an increase in the Weissenberg number.

REFERENCES

1. Ariel PD, Axisymmetric Flow of a Second Grade Fluid Past a Stretching Sheet, Intern. J. Engng Sci., 39, 529–553 (2001).
2. Ariel PD, Axisymmetric Flow due to a Stretching Sheet with Partial Slip, Comput. Math. Appl., 54, 1169–1183 (2007).
3. Sahoo B, Effects of Partial Slip on Axisymmetric Flow of an Electrically Conducting Viscoelastic Fluid Past a Stretching Sheet, Centr. Eur. J. Phys. 8 (3), 498–508 (2010).
4. Shahzad A, Ali R, and Khan M, On the Exact Solution for Axisymmetric Flow and Heat Transfer over a Non-Linear Radially Stretching Sheet, Chinese Phys. Lett. 29, 084705 (2012).
5. Ali R, Shahzad A, Khan M, and Ayub M, Analytical and Numerical Solutions for Axisymmetric Flow with Partial Slip, Engng Comput. 32 (1), 149–154 (2016).
6. Bird RB, Curtiss CF, Armstrong RC, and Hassager O, Dynamics of Polymeric Liquids, Wiley, New York, 1987.
7. Carreau PJ, Rheological Equations from Molecular Network Theories, Trans. Soc. Rheol. 116, 99–127 (1972).
8. Chhabra RP and Uhlherr PHT, "Creeping Motion of Spheres Through Shear-Thinning Elastic Fluids Described by the Carreau Viscosity Equation," Rheol. Acta. 19, 187–195 (1980).
9. Bush MB and Phan-Thein N, Drag Force on a Sphere in Creeping Motion Through a Carreau Model Fluid, J. Non-Newtonian Fluid Mech. 16, 303–313 (1984).
10. Khan M and Hashim, Axisymmetric flow and heat transfer of the Carreau fluid due to a radially stretching sheet: numerical study, Journal of Applied Mechanics and Technical Physics, 2017, 58(3), 410–418.
11. Hussanan A, Salleh MZ, Khan I, Tahar RM (2016) Heat and mass transfer in a micropolar fluid with Newtonian heating: an exact analysis. Neural Comput Appl. doi:10.1007/s00521-016- 2516-0

12. Rashidi MM, Momoniat E, Rostami B (2012) Analytic approximate solutions for MHD boundary-layer viscoelastic fluid flow over continuously moving stretching surface by homotopy analysis method with two auxiliary parameters. J Appl Math. doi:10.1155/2012/780415
13. Rashidi MM, Ali M, Rostami B, Rostami P, Xie GN (2015) Heat and mass transfer for MHD viscoelastic fluid flow over a vertical stretching sheet with considering Soret and Dufour effects. Math Probab Eng 2015:861065
14. Ashraf MB, Hayat T, Alsaedi A, Shehzad SA (2015) Convective heat and mass transfer in MHD mixed convection flow of Jeffrey nanofluid over a radially stretching surface with thermal radiation. J Cent South Univ 22(3):1114–1123
15. Shehzad SA, Alsaadi FE, Monaquel SJ, Hayat T (2013) Soret and Dufour effects on the stagnation point flow of Jeffery fluid with convective boundary condition. Eur Phys J Plus 128:56
16. Ibrahim W, Haq RU (2016) Magnetohydrodynamic (MHD) stagnation point flow of nanofluid past a stretching sheet with convective boundary condition. J Braz Soc Mech Sci 38(4):1155–1164
17. Rahman MM, Rosca AV, Pop I (2015) Boundary layer flow of a nanofluid past a permeable exponentially shrinking surface with convective boundary condition using Buongiorno's model. Int J Numer Methods Heat Fluid Flow 25(2):299–319
18. Ramzan M, Farooq M, Hayat T, Chung JD (2016) Radiative and Joule heating effects in the MHD flow of a micropolar fluid with partial slip and convective boundary condition. J Mol Liq 221:394–400
19. Waqas M, Farooq M, Khan MI, Alsaedi A, Hayat T, Yasmeen T (2016) Magnetohydrodynamic (MHD) mixed convection flow of micropolar liquid due to nonlinear stretched sheet with convective condition. Int J Heat Mass Transf 102:766–772
20. Ramzan M, Bilal M, Chung JD and Mann AB, (2017), On MHD radiative Jeffery nanofluid flow with convective heat and mass boundary conditions, Neural Comput & Applic., DOI 10.1007/s00521-017-2852-8